THE JOURNAL OF PHYSICAL CHEMISTRY C

ARTICLE

pubs.acs.org/JPCC

Structural Study of D_2 within the Trimodal Pore System of a Metal Organic Framework

Vanessa K. Peterson,[*,†] Craig M. Brown,[‡] Yun Liu,[‡,§] and Cameron J. Kepert[∥]

[†]The Bragg Institute, Australian Nuclear Science and Technology Organisation, Locked Bag 2001, Kirrawee DC, NSW 2232, Australia

[‡]National Institute of Standards and Technology Center for Neutron Research, Gaithersburg, Maryland 20899-8562, United States

[§]Department of Chemical Engineering, University of Delaware, Newark, Delaware 19716, United States

[∥]School of Chemistry, The University of Sydney, NSW 2006, Australia

S *Supporting Information*

ABSTRACT: D_2 loaded to saturation at 25 K into the porous coordination framework Cu_3(1,3,5-benzenetricarboxylate)$_2$ was studied using neutron powder diffraction. A saturation loading equivalent to 6.1 wt % H_2 is reached at 25 K. D_2 is located at up to nine distinct sites with six stable at saturation and three "metastable" sites at doses intermediate to saturation. Filling of the trimodal pore system is complex, and a concentration dependency on the optimal D_2 arrangement is noted. A dynamic rearrangement of the D_2 in the pores to a cubic-closed packed equilibrium structure occurs at doses close to saturation, with 4 D_2 molecules arranged tetrahedrally in the smallest pore, 32 D_2 arranged in a truncated octahedron with capped hexagonal faces in the intermediate sized pore, and 48 D_2 arranged in a face-capped rhombic dodecahedron in the largest pore. The equilibrium structure of D_2 in the largest pore at doses close to and at saturation was found to be the same arrangement that is optimal for 48 circles on a sphere. The structural response of the framework to D_2 adsorption is dependent on the amount of D_2, where the host lattice expands with increasing amount of adsorbed D_2 at low and high D_2 doses, and contracts upon adsorption of intermediate amounts of D_2, commensurate with the known flexibility exhibited by this framework.

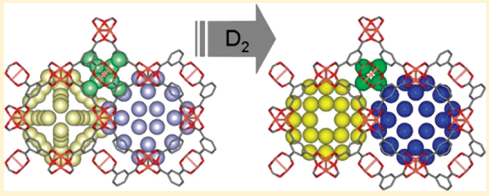

INTRODUCTION

Porous framework complexes are at the forefront of research as materials with properties useful in applications such as gas-storage,[1−14] catalysis,[2,5,15−20] sensing,[3,21,22] and separations.[5,10,11,18,23−25] Understanding the structure−function relationships of these materials, particularly the structural response of the framework, is paramount to advancing toward materials with superior properties for these and new functions. As new materials are created and examined for these purposes, new properties are uncovered such as negative thermal expansion[26−29] and guest-dependent lattice expansion.[30]

This study considers the three-dimensional porous framework material, $Cu_3(BTC)_2$,[31] where BTC = 1,3,5-benzenetricarboxylate, which has several features of interest, most notably a topology that gives rise to a range of pore sizes and dimeric Cu units, connected to four BTC units, each with two coordinatively unsaturated Cu sites. $Cu_3(BTC)_2$ has a range of properties shown useful for catalysis,[32,33] surface and molecular selection and separations,[32,34−41] and storage of hydrogen and other gases.[12,37,38,42−51] Other properties of this material have been identified and studied, including cooperative magnetic behavior[52−54] and flexibility that results in a new mechanism of negative thermal expansion,[28,29] also studied *via* the material's response to pressure.[30] Furthermore, the range of properties of this remarkable material has raised interest in the methods and mechanism of its formation.[33,37,43,55−61]

$Cu_3(BTC)_2$ contains several features that allow exploration of the material−dihydrogen interaction, including the coordinatively unsaturated Cu that provides a binding site for H_2.[45,47,62] The overall framework is neutral; however, a partial positive charge is found at the Cu atoms with the remaining partial negative charges localized on the carboxylate units.[48] The electron-delocalization at the benzene units provides possible dihydrogen binding *via* Coloumb-type electrostatic interactions. Finally, the structure exhibits a complex trimodal pore distribution, with a topology resulting in connectivity between some but not all of the pores. We use a description of the three pores as follows. Pore "A" is cuboctahedral and approximately 10.7 Å across (distance between Cu atoms of opposite dimeric units), formed from 12 $Cu_2(OOC)_4$ units and containing face-on benzene linker units. Pore A is connected to a secondary pore system, pore "B", centered on the faces and corners of the unit cell with a distance across the pore center of approximately 12.7 Å (distance between Cu atoms of opposite dimeric units). Pore B is connected *via* triangular windows to the smallest pores, pore "C", in which four benzene rings constitute the inner surface with the centers of the rings forming a tetrahedron approximately 5 Å in diameter. The BTC units make pore C inaccessible from pore A.

Received: February 1, 2011
Revised: March 24, 2011
Published: April 12, 2011

Previous work investigated D_2 adsorption in $Cu_3(BTC)_2$ to a concentration of 4 wt %, achieved at 25 K, using neutron powder diffraction. A progressive filling of six distinct D_2 sites, labeled $D_2(1)$ up to $D_2(6)$ in order of appearance, up to the 4 wt % concentration was found. The primary site, $D_2(1)$, was noted at the coordinatively unsaturated Cu atoms. A progressive filling of the smallest pore (C) followed by the larger pore (A) was noted. A subsequent inelastic neutron scattering study of H_2 in the system showed three binding sites that are progressively populated when the H_2 loading is less than 2.0 H_2:Cu, consistent with the neutron powder diffraction results.[45] The inelastic scattering study estimated the H_2 adsorption enthalpy of the $H_2(1)$, $H_2(2)$, and $H_2(3)$ to be between 6 and 10 kJ/mol, approximately 5−6 kJ/mol, and less than 5 kJ/mol, respectively. Subsequent inelastic neutron scattering and first-principles modeling revealed that the form factors of the three main rotational peaks follow that expected for a free hydrogen molecule with a regular H−H intramolecular bond distance, although the orientation potential at the Cu-adsorption site is slightly two-dimensional, with a tendency for the H_2 to lie in a plane perpendicular to the Cu−Cu bond.[62]

Within pore C, filling of the sites is highly competitive, and a complex response of the framework and D_2−D_2 interaction within pore C and pore A was revealed. The appearance of the $D_2(5)$ site was found to stabilize the concentration of D_2 at the $D_2(2)$ site, which saturated at a site occupancy factor (SOF) of 0.16 D_2 per Cu. An inspection of the $D_2 \cdots D_2$ site distances revealed a fluxional site occupation within pore C, and at the 4 wt % loading, the refined site occupancies were consistent with *ca.* 20% of pores C containing two D_2, at the $D_2(2)$ site, and *ca.* 80% containing three D_2, two D_2 at the $D_2(5)$ site, and one at the $D_2(2)$ site. In addition to the D_2 site competition, the crystalline lattice of the $Fm\bar{3}m$ (*a* is approximately 26.4 Å) structure changes during D_2 adsorption, expanding initially as D_2 is adsorbed, then contracting at D_2:Cu loadings of 2 and 4. This contraction is associated with a subtle buckling of the BTC units and a concomitant decrease in the BTC bridged Cu···Cu distance from 8.07(1) to 8.03(1) Å.

The framework response to D_2 adsorption and its effect on D_2 adsorption becomes increasingly important during higher D_2 loadings. This work explores D_2 occupation and location in $Cu_3(BTC)_2$ at high D_2:Cu loadings, and in particular the competitive D_2 site filling in the trimodal pore system.

EXPERIMENTAL METHODS

Preparation of $Cu_3(BTC)_2$. $Cu_3(BTC)_2$ was prepared as described elsewhere.[28,29,47] A 0.04883 mol portion of $Cu(NO_3)_2 \cdot 3H_2O$ was dissolved in 42 mL of H_2O and added to 0.02457 mol of H_3BTC dispersed by sonication in 42 mL of ethanol and stirred for 20 min. The mixture was divided into seven 20 mL Teflon inserts, placed in Parr solvothermal bombs, and heated to 95 °C for 18 h. The solid was sonicated with methanol for 20 min, heated to 40 °C, and the liquid decanted. The washing and heating processes were repeated until phase-pure octahedral blue crystals were observed by optical microscopy. Dehydration (activation) of the sample from $Cu_3(BTC)_2(H_2O)_3$ to $Cu_3(BTC)_2$ was performed in a glass tube with a packless bellows valve attached. The sample was evacuated using a turbo pump (10^{-3} Pa), heated at 1 °C/min to 150 °C, and degassed for 24 h.

Sample Preparation and Neutron Powder Diffraction. Prior to neutron powder diffraction measurement and D_2 dosing, activated $Cu_3(BTC)_2$ was further degassed *in situ* for *ca.* 20 min under high vacuum (1.1×10^{-4} to 1.0×10^{-3} Pa) at 150 °C. The activated sample was transferred to a cylindrical vanadium can (internal diameter ≈0.95 cm) equipped with a capillary gas line and a packless valve in a helium-filled glovebox equipped with water and oxygen monitors, and sealed with an indium O-ring. The sample was mounted onto a sample stick equipped with a stainless-steel gas line with an additional valve for a top-loading closed-cycle helium refrigerator. Neutron powder diffraction data were collected on the high-resolution neutron powder diffractometer BT-1 at the National Institute of Standards and Technology (NIST) Center for Neutron Research (NCNR) with a Ge(311) monochromator and using in-pile 15 arc minute collimation, corresponding to a wavelength of 2.0787 Å. After the initial $Cu_3(BTC)_2$ measurement at 3.5 K, gas loaded measurements were taken as a function of D_2 loading with all measurements at a temperature of 3.5 K. The loading of known amounts of D_2 gas into the sample (2.896 g) corresponding to D_2:Cu ratios of 0, 3.1, 4.5, 4.9, 5.6, and 6.6 was performed at temperatures ranging from 55 K at low coverage to 30 K for the highest loading. The sample was cooled to 3.5 K over 1 h to ensure diffusion of the D_2 to its equilibrium location within the sample and neutron powder diffraction data collected for D_2-loaded $Cu_3(BTC)_2$.

Structural Analysis. Rietveld refinements were performed using GSAS as implemented in EXPGUI.[63,64] Rietveld refinement was performed using the structural model for the bare $Cu_3(BTC)_2$,[31] with atoms in the asymmetric unit redefined to lie within a single unit cell. A 16-term shifted Chebyschev background function and the pseudo-Voigt peak profile with asymmetry (CW Type III in GSAS) was used. The resulting crystalline model for the bare framework was used for the analyses of the powder diffraction data of $Cu_3(BTC)_2$ and then as the initial model for the D_2 adsorbed data with the D_2 locations derived using Fourier difference techniques. Three small reflections from the bare framework (appearing also in the D_2-loaded material) were unable to be indexed by the model. These reflections were attributed to impurities in the sample. Given the high affinity of the framework for D_2 and the small phase fraction of this contaminant phase, it is unlikely that this contaminant affects the measured D_2 sorption significantly. These additional reflections were removed from the fitting procedure, with excluded regions incorporated from 2θ = 59.65−60.35°, 70.45−71.10°, and 109.65−110.75°. All reflections arising in the presence of the gas-loaded framework were able to be indexed using the $Fm\bar{3}m$ space group. This corrected "bare" model was used as a baseline for all subsequent measurements involving D_2. In each case, the model for the bare framework was refined before the Fourier difference was taken to identify the guest molecules. Deuterium molecules are treated as point scatterers with double occupancy. The D_2 locations and occupancy were then obtained by Rietveld refinement. The D_2−D_2 distances were considered in conjunction with the SOFs in order to check that physically realistic results for D_2 location were obtained in cases where local disorder of D_2 arrangement in the pores was present, as noted in previous work.[47]

RESULTS AND DISCUSSION

Rietveld refinement using neutron powder diffraction data (Figure 1 and Table S1 in the Supporting Information) revealed the location of nine distinct D_2 sites located in $Cu_3(BTC)_2$. All

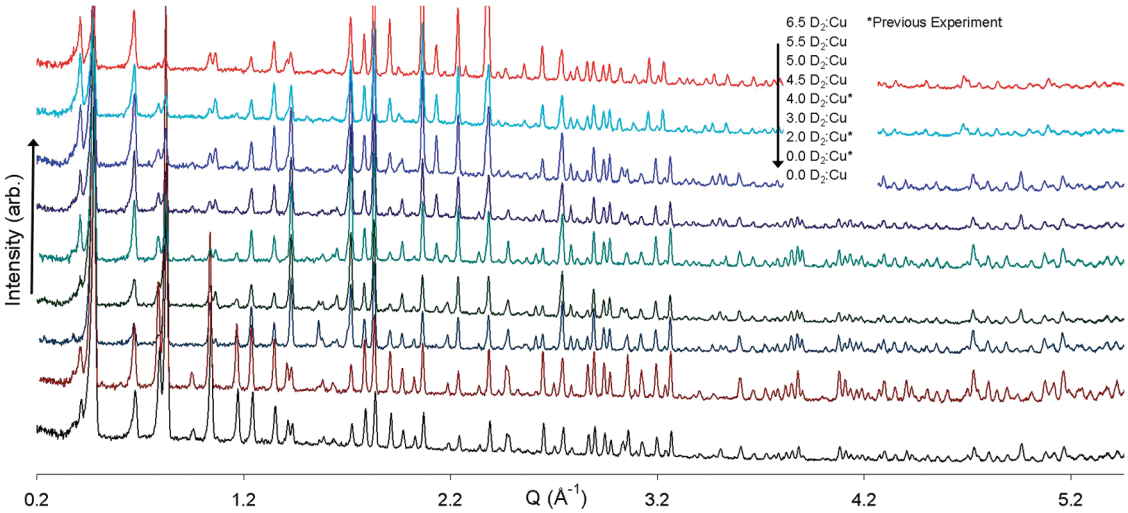

Figure 1. Neutron powder diffraction data of $Cu_3(BTC)_2$ loaded with D_2 from this and previous[47] work.

Table 1. Site, Site Occupancy Factor (SOF), and Isotropic Atomic Displacement Parameter (ADP) for Each D_2 in $Cu_3(BTC)_2$[a]

		$D_2(1)$	$D_2(2)$	$D_2(3)$	$D_2(4)$	$D_2(5)$	$D_2(6)$	$D_2(7)$	$D_2(8)$
D_2:Cu		pore B	pore C	pore C/B	pore A	pore C	pore A	pore B	pore A
3	SOF	0.97(2)	0.96(4)		0.38(2)	0.50(3)	0.20(2)		
					D_2(4a)				
	ADP, Å^2	0.125(3)	0.23(1)		0.14(1)	0.62(6)	0.43(5)		
4.5	SOF	0.92(1)	0.26(4)	0.71(4)	0.49(3)	0.79(2)	0.38(3)	0.17(2)	
					(D_2(4a))				
	ADP, Å^2	0.127(4)	0.13(2)	0.23(2)	0.24(2)	0.24(1)	0.27(2)	0.37(7)	
	SOF				0.42(2)				
					(D_2(4b))				
	ADP, Å^2				0.18(1)				
5	SOF	0.77(1)		0.94(5)	0.23(2)	1.02(3)	0.21(2)	0.28(2)	
					(D_2(4a))				
	ADP, Å^2	0.085(4)		0.19(1)	0.12(2)	0.27(1)	0.23(3)	0.24(2)	
	SOF				0.69(3)				
					(D_2(4b))				
	ADP, Å^2				0.21(1)				
5.5	SOF	0.87(2)		1.08(3)	1.06(2)	0.95(2)		0.46(1)	0.52(2)
					(D_2(4b))				
	ADP, Å^2	0.108(4)		0.24(1)	0.26(1)	0.16(1)		0.24(1)	0.11(1)
6.5	SOF	0.95(2)		1.04(2)	0.99(1)	0.92(2)		0.84(1)	1.04(2)
					(D_2(4b))				
	ADP, Å^2	0.120(4)		0.23(1)	0.146(3)	0.17(1)		0.17(1)	0.16(1)

[a] Values in parentheses are estimated standard deviations in the last significant figure.

D_2 introduced into the sample was accounted for by the Rietveld model, with exceptional agreement between the dosed and calculated D_2 concentrations (Table S1, Supporting Information). The following sections will focus on the loading characteristics by describing the adsorption sites and the structural rearrangements observed, followed by a detailed examination of the saturation structure of the deuterium, and finally the effect that loading has on the framework itself.

D_2 Adsorption Sites in $Cu_3(BTC)_2$. Our previous work[47] included loadings of up to 4 D_2:Cu in $Cu_3(BTC)_2$ and identified 6 D_2 binding sites. This earlier work considered D_2 with respect to the Cu site, pore C (smallest), and pore A (the intermediate sized aromatic pore), since the adsorbed D_2 was related by symmetry to those located in the largest pore, B. At higher D_2 doses, as applied here, sites additional to those previously identified are located in the largest pore, B. Table S2 (Supporting Information) lists the nine distinct sites for D_2 within $Cu_3(BTC)_2$, and Table 1 reports the site occupancy factor (SOF) and atomic displacement parameter (ADP) for each D_2 site at various D_2:Cu loadings (Figure 2).

The most favorable site, $D_2(1)$, occupies the coordinatively unsaturated axial sites of the dinuclear Cu centers, as noted

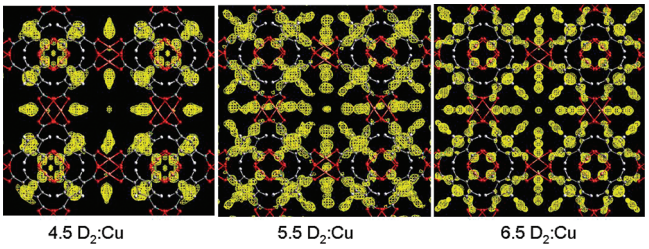

Figure 2. Fourier-difference maps shown along [001] for the unit cell featuring nuclear scattering density arising from D_2 (yellow) in $Cu_3(BTC)_2$ at a density of 0.7 fmÅ^{-3} from three different D_2 doses (increasing left to right). Shown are Cu (metallic copper), O (red), C (gray), and H (white).

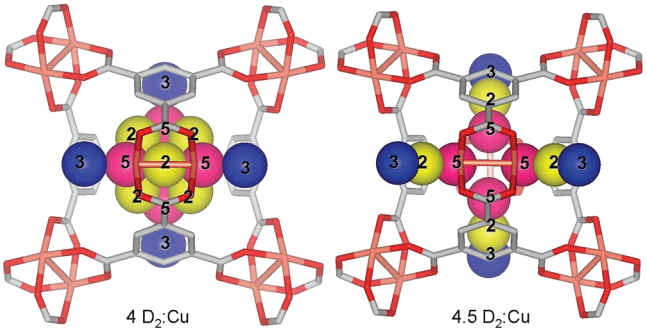

Figure 3. Rearrangement of D_2 in pore C, at low[47] and high D_2 loadings. Adsorption sites are labeled and colored according to sites described in the text. For clarity, framework H atoms are not shown.

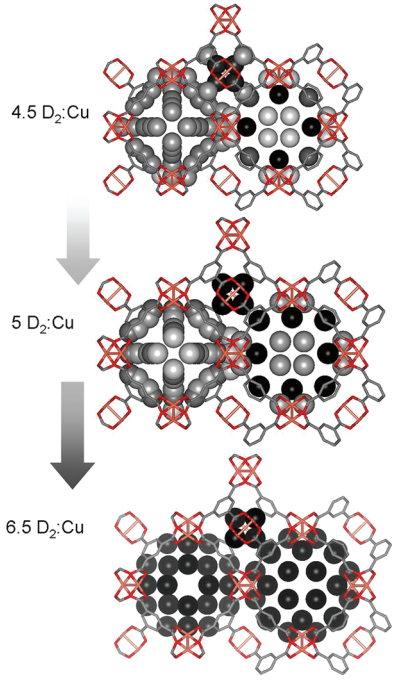

Figure 4. D_2 arrangement at the 4.5 (top), 5.5 (middle), and 6.5 (bottom) D_2:Cu doses. The framework is shown with O (red), C (gray), and Cu (pink dimeric units). D_2 sites are shown as circles with occupancy indicated in grayscale intensity (black = 1). For clarity, H's are omitted and the $D_2(6)$ site is shown only at the front and left views in pore A.

previously. Here, we report a decrease of up to 23% of D_2 at $D_2(1)$ at doses intermediate to saturation. Given that all D_2 is accounted for by the model, we attribute this to some "trapping" of the D_2 at the nonequilibrium position during the data collection that highlights the fluxional nature of the adsorbed hydrogen and the likely dependence on the loading/cooling protocols.

Pore C, the smallest pore, is the next place that D_2 is adsorbed into, with our earlier work showing that the second site, $D_2(2)$, is populated before saturation of the primary $D_2(1)$ site.[47,62] Subsequent population of the pore C window sites, $D_2(3)$, occurs followed by population of the $D_2(5)$ site, located near the center of the smallest pore. For reasons that will be explained later, where we previously[47] labeled the centroids of the pore C sites as $D_2(2)$ at (0.25, 0.25, 0.34) and $D_2(3)$ at (0.16, 0.16, 0.16), they are now relabeled as $D_2(2)$ at (0.17, 0.17, 0.17) and $D_2(3)$ at (0.138, 0.138. 0.138). The four $D_2(2)$ sites are arranged tetrahedrally with respect to each other in a similar fashion to the $D_2(5)$ site, with all four $D_2(2)$ sites (*ca.* 6 Å apart) and all four $D_2(5)$ sites able to be occupied (*ca.* 3 Å apart) simultaneously, unlike the previous assignment where at most two of the six possible octahedrally arranged $D_2(2)$ sites could be occupied. While the neighboring $D_2(2)$ and $D_2(5)$ sites are likely both occupied at 3 D_2:Cu loading resting *ca.* 2.5 Å apart, at 4.5 D_2:Cu these sites approach each other to *ca.* 1.8 Å, a distance so short that they cannot be simultaneously occupied. While these sites jostle, a shift of the $D_2(3)$ site away from the $D_2(5)$ site at higher D_2 dosages occurs. The initial low-dose location of $D_2(3)$ at the window entrance to pore C shifts to just inside pore B with further loadings. This alternative description of the adsorption sites results in the $D_2(3)$ site being approximately 1.4 Å away from the $D_2(2)$ site, compared to 3.6 Å in the previous description. Site population occurs in the order of $D_2(2)$, then $D_2(5)$, followed by the $D_2(3)$ site. The fact that these two adsorption sites are derivatives of each other is likely; the population of $D_2(3)$ begins when there is depopulation at the $D_2(2)$ site. The $D_2(2)$ site is completely depopulated at D_2 dosages greater than 4.5 D_2:Cu, leaving 4 D_2 molecules in the smallest pore at saturation occupying the $D_2(5)$ position.

The interaction of D_2 in the confines of the smallest pore results in a significant repositioning of the optimal $D_2(5)$ location between the 3 D_2:Cu and the 4.5 D_2:Cu loads (Table S2, Supporting Information). Locally, D_2 at the $D_2(5)$ site may be positioned at either of these locations, depending on the local concentration of D_2 in that particular pore. This effect is reflected in the significantly higher ADP of 0.62(6) for the $D_2(5)$ in the 3 D_2:Cu load, before reducing to the more modest ADP of 0.24(1) in the 4.5 D_2:Cu load, where there is *ca.* 50% more D_2 at the $D_2(5)$ site.

Within the larger pore system, two sites were identified at lower loadings, the $D_2(4)$ and $D_2(6)$ sites, both located in the aromatic pore, A. The higher adsorption values measured here show that the $D_2(6)$ site is transitional in nature, and disappears with D_2 loadings in a similar fashion to $D_2(2)$. Shifting of the previously labeled $D_2(4)$ site with higher loadings warrants a relabeling of this site as $D_2(4a)$. While $D_2(4a)$ appears only at loadings of 5 D_2:Cu and below, it smears across the higher multiplicity site $D_2(4b)$ at the 4.5 D_2:Cu load, most likely representing a variety of local arrangements of D_2 in this pore. The $D_2(4a)$ site is similarly positioned between the 3.5, 4.5, and 5 D_2:Cu loads; however, at the 4.5 D_2:Cu load, the exact position of the D_2 results in a different site multiplicity. The $D_2(4a)$ site is

approximately 1.7 Å from the $D_2(6)$ site. Therefore, these three sites are mutually exclusive and nearby sites cannot be occupied at the same time. The $D_2(4a)$ site is transitional in nature and gives way for further population of the final $D_2(4b)$ site. Further loading to 5.5 D_2:Cu gives rise to adsorption at $D_2(8)$ and a remarkable transition of the packing of D_2 inside pore A to a cubic closed-packed arrangement, with the exception of 7 "absent" D_2 molecules at the center, resulting in this pore being occupied by 32 D_2 molecules. This arrangement remains at the highest loading, 6.5 D_2:Cu. No more D_2 than this loading was able to be adsorbed by the sample held at 25 K.

Pore B has one additional adsorption site, $D_2(7)$, besides the two sites described above as $D_2(1)$, the coordinatively unsaturated Cu^{2+}, and $D_2(3)$, that migrates from within the window of pore C. The appearance of the third and final site in this pore occurs at 4.5 D_2:Cu at the same time that $D_2(3)$ migrates. Residing just 1.9 Å from $D_2(6)$ in the adjacent pore A, the $D_2(6)$ site depopulates commensurately with increasing population of the $D_2(7)$ site; the $D_2(6)$ site disappears at the 5.5 D_2:Cu loading. At saturation, 48 D_2 molecules are present in pore B. Interestingly, there is no change in the arrangement of the sites in the largest pore unlike the dramatic rearrangement of the D_2 sites in pore A.

The intermolecular separations for D_2 in $Cu_3(BTC)_2$ are relatively short, most notably the neighboring $D_2(2)$ and $D_2(5)$ sites (both occupied) at the 3 D_2:Cu loading that rest *ca.* 2.5 Å apart. These short distances are consistent with other reports of D_2 adsorption in porous framework materials, as discussed in recent work[65] commenting on previous findings of a 2.85 Å D_2-D_2 separation in MOF-74-Zn.[66] Similar findings for H_2 in H_2-hydrates are noted,[67] where H_2 forms a tetrahedron with only 2.42−2.53 Å between the H_2 at the cage center and the corner H_2.

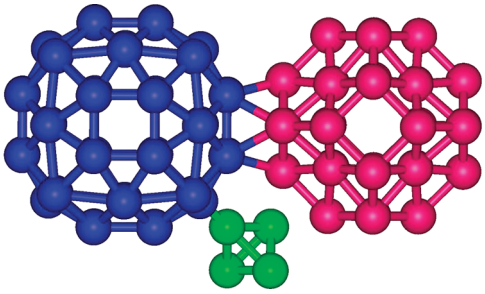

Figure 5. Arrangement of D_2 in the three pores. D_2 are represented as spheres and shown green in the smallest pore (C), pink in the large aromatic pore (A), and blue in the largest pore (B).

Final Arrangement of D_2 at Saturation. The final arrangement of D_2 loaded to saturation at 25 K is distinctly different in each of the three pores (Figure 5). In the smallest pore, C, four D_2 molecules form a regular tetrahedron, where the $D_2 \cdots D_2$ centroid distance is approximately 3.25 Å. This pore connects to the largest pore, pore B, where 48 D_2 molecules are located at the vertices of a face-capped truncated rhombic dodecahedron; the same packing arrangement is optimal for 48 circles on a sphere.[68] In the medium-sized pore, A, 32 D_2 molecules form a truncated octahedron with capped hexagonal faces. The three $D_2 \cdots D_2$ distances in pore B are 3.2, 3.7, and 3.4 Å, and in pore A, these are 3.4, 3.4, and 3.5 Å. Interestingly, pore A contains apparently open space at the loading level we obtained at 25 K. Further loading and cooling down to 16 K might alter this arrangement and increase the capacity, as noted in MOF-5, where a similar close-packed arrangement was noted.[69] The space located at the center of pore A could accommodate an additional 7 D_2 molecules. If these 7 sites were able to be fully occupied, this would correspond to 7.58 D_2 per Cu (the equivalent of 7.0 wt % H_2).

The dynamic rearrangement of the D_2 in the pores at saturation results in an essentially even monolayer distribution of the D_2 around the inner pore surface (with the exception of the $D_2(1)$) with D_2 molecules roughly equidistant. In pore C, the centroid of the $D_2(5)$ site is *ca.* 3.9 Å from the closest part of the framework but only 3.1 Å from $D_2(3)$ in pore B. In pore A, the $D_2(4b)$ site is *ca.* 3.5 Å from the framework and $D_2(8)$ is *ca.* 3.6 Å from the framework, with $D_2(4b)$ 3.5 Å from $D_2(7)$ in pore B. The closest D_2 comes toward the framework is in pore B where $D_2(1)$ docks only *ca.* 2.4 Å from the Cu^{II} ion. The $D_2(7)$ site in pore B is arranged at a distance intermediate to the shorter $D_2(1)$ distance and that of the other sites, at 2.6 Å. The final site in this pore, $D_2(3)$, is 3.4 Å from the framework but only 3.1 Å from $D_2(5)$. With the exception of the $D_2(1)$ site, the D_2 arranges itself as evenly as possible with respect to the framework surface and to other D_2 molecules. The slightly stronger affinity of D_2 to the unsaturated metal center than to the framework is consistent with the reported nature of the hydrogen phase in several

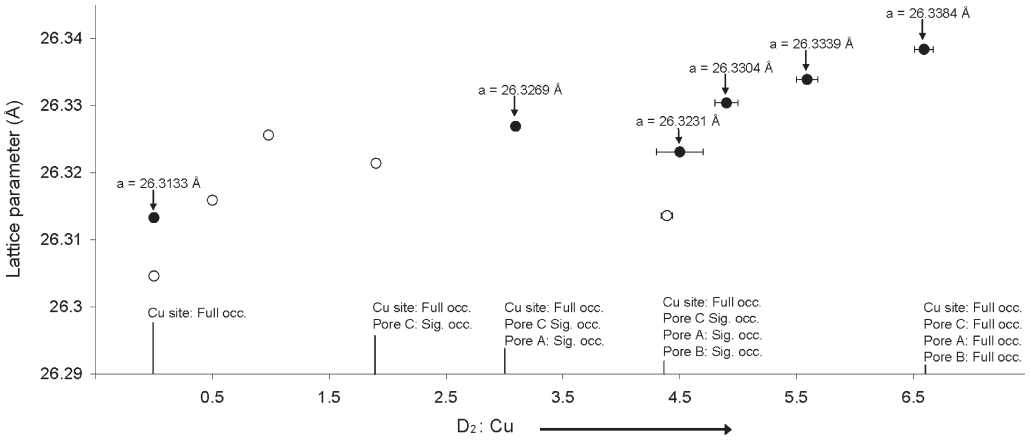

Figure 6. $Cu_3(BTC)_2$ cubic lattice-parameter response to D_2 adsorption. Shown are lattice parameters from this (closed circles) and a previous[47] (open circles) study. Arrows and text indicate D_2 occupation at the Cu site and at sites within the three pores at various D_2:Cu doses (Full occ., fully occupied; Sig. occ., significantly occupied).

moderately weak adsorption enthalpy metal organic frameworks, and in this case, the chemical composition of the adsorbent is not altered much by differences in the sample's affinity for molecular hydrogen. This does not address the case where there is a stronger enthalpy of adsorption and the mean distance between next-neighbor D_2 is smaller than in the bulk solid, resulting in a denser packing,[66] as demonstrated by the observation of liquid-like hydrogen observed in porous coordination frameworks.[70]

Framework Response to D_2 Adsorption. The most notable crystal structure change in $Cu_3(BTC)_2$ upon D_2 adsorption occurs to the unit-cell dimension that varies according to the quantity of D_2 adsorbed (Figure 6) and the subsequent structural arrangement of the adsorbate. The unit cell initially expands linearly for doses below 1 D_2:Cu followed by a slight contraction when amounts of D_2 ranging from 2 to 4.5 D_2:Cu are adsorbed. We previously[47] associated this with a subtle buckling of the BTC units and a concomitant decrease in the BTC bridged Cu−Cu distance from 8.07(1) to 8.03(1) Å. The response of the unit cell becomes positive and more linear at D_2 loadings above 5 D_2:Cu. A careful examination of the D_2 sites (Table 2) reveals that the unit-cell response is correlated with increasing population at specific D_2 guest sites.

Most notably, the contraction of the lattice observed at D_2 doses of approximately 4.5 D_2:Cu is associated with significant disorder in pore A. It is above this loading that the D_2(4a) site becomes less distinct, smearing into the D_2(8) and D_2(4b) sites. A similar situation exists for D_2 in the other two pores, with two exceptions: the D_2 at site D_2(2), in pore C, and at D_2(6), in pore A. We attribute the lattice response to significant occupation of D_2 in the large aromatic pore, A, at the D_2(6) site. This site is intermediate in nature and begins to depopulate at the 5 D_2:Cu dose (with increasing population of the D_2(4b) site). This site is located in the large pore entrance, where four dimeric units form the corners of the large pore boundary. D_2(6) is approximately 4.07 Å equidistant from the closest Cu atom of each dimer. The apparent reduction in the lattice at intermediate D_2 doses is not unexpected given the known flexibility of this framework, as demonstrated by its negative thermal expansion.[28,29]

CONCLUSIONS

We observe D_2 adsorption in a trimodal porous metal organic framework, $Cu_3(BTC)_2$, up to saturation at 25 K using neutron powder diffraction. Saturation is reached at a loading of 6.5 D_2:Cu, corresponding to the equivalent of 6.1 wt % H_2. The D_2 is located at up to nine distinct sites, with six stable at saturation, and three sites that are metastable and exist at intermediate doses. The pore filling follows a complex mechanism, with D_2 sites changing between D_2 dosages, arising as a result of concentration-dependent optimal D_2 arrangements caused by D_2−D_2 and D_2−framework interactions. At saturation, one site exists in the smallest pore, two in the intermediate sized pore, and three in the largest pore. Most notably, a dynamic transition to a high symmetry D_2 arrangement is observed at doses approaching saturation. In this arrangement, the smallest pore contains 4 D_2 arranged tetrahedrally and the intermediate sized pore contains 32 D_2 arranged in a truncated octahedron with capped hexagonal faces. Interestingly, the largest pore contains 48 D_2 arranged in a face-capped rhombic dodecahedron, the same arrangement that has been shown to be optimal for 48 circles on a sphere. The arrangement of D_2 at saturation has D_2 molecules roughly equidistant from each other and from the framework surface, with the exception of the strongest binding site, located at the coordinatively unsaturated Cu^{II} ions, which are closer. The framework responds structurally to the adsorption of D_2, expanding at low and high D_2 doses, although at intermediate doses the framework lattice displays an apparent reduction upon population of the metastable D_2 sites, a behavior that is commensurate with the known flexibility of the material.

ASSOCIATED CONTENT

Supporting Information. Figure of merit (wR_p) for Rietveld analysis using neutron diffraction data for $Cu_3(BTC)_2$ loaded with D_2 as well as D_2 quantities and site locations obtained from the refinements. This material is available free of charge via the Internet at http://pubs.acs.org.

AUTHOR INFORMATION

Corresponding Author
*E-mail: vanessa.peterson@ansto.gov.au.

ACKNOWLEDGMENT

Work at NIST was partially supported by the U.S. DOE within the Hydrogen Sorption Center of Excellence. C.J.K. acknowledges the Donors of the American Chemical Society Petroleum Research Fund for partial support of this research.

REFERENCES

(1) Banerjee, R.; Phan, A.; Wang, B.; Knobler, C.; Furukawa, H.; O'Keeffe, M.; Yaghi, O. M. *Science* **2008**, *319*, 939–943.
(2) Cheetham, A. K.; Rao, C. N. R. *Science* **2007**, *318*, 58–59.
(3) Chen, B.; Wang, L.; Zapata, F.; Qian, G.; Lobkovsky, E. B. *J. Am. Chem. Soc.* **2008**, *130*, 6718–6719.
(4) Dinca, M.; Long, J. R. *J. Am. Chem. Soc.* **2007**, *129*, 11172–11176.
(5) Farha, O. K.; Mulfort, K. L.; Thorsness, A. M.; Hupp, J. T. *J. Am. Chem. Soc.* **2008**, *130*, 8598–8599.
(6) Farha, O. K.; Spokoyny, A. M.; Mulfort, K. L.; Hawthorne, M. F.; Mirkin, C. A.; Hupp, J. T. *J. Am. Chem. Soc.* **2007**, *129*, 12680–12681.
(7) Luo, J.; Xu, H.; Liu, Y.; Zhao, Y.; Daemen, L. L.; Brown, C.; Timofeeva, T. V.; Ma, S.; Zhou, H.-C. *J. Am. Chem. Soc.* **2008**, *130*, 9626–9627.
(8) McKinlay, A. C.; Xiao, B.; Wragg, D. S.; Wheatley, P. S.; Megson, I. L.; Morris, R. E. *J. Am. Chem. Soc.* **2008**, *130*, 10440–10444.
(9) Mulfort, K. L.; Hupp, J. T. *J. Am. Chem. Soc.* **2007**, *129*, 9604–9605.
(10) Noguchi, D.; Tanaka, H.; Kondo, A.; Kajiro, H.; Noguchi, H.; Ohba, T.; Kanoh, H.; Kaneko, K. *J. Am. Chem. Soc.* **2008**, *130*, 6367–6372.
(11) Wang, B.; Cote, A. P.; Furukawa, H.; O'Keeffe, M.; Yaghi, O. M. *Nature* **2008**, *453*, 207–U206.
(12) Xiao, B.; Wheatley, P. S.; Zhao, X.; Fletcher, A. J.; Fox, S.; Rossi, A. G.; Megson, I. L.; Bordiga, S.; Regli, L.; Thomas, K. M.; Morris, R. E. *J. Am. Chem. Soc.* **2007**, *129*, 1203–1209.
(13) Yang, C.; Wang, X.; Omary, M. A. *J. Am. Chem. Soc.* **2007**, *129*, 15454–15455.
(14) Sumida, K.; Horike, S.; Kaye, S. S.; Herm, Z. R.; Queen, W. L.; Brown, C. M.; Grandjean, F.; Long, G. J.; Dailly, A.; Long, J. R. *Chem. Sci.* **2010**, *1*, 184−191.
(15) Chan, B.; Radom, L. *J. Am. Chem. Soc.* **2008**, *130*, 9790–9799.
(16) Han, J. W.; Hill, C. L. *J. Am. Chem. Soc.* **2007**, *129*, 15094–15095.
(17) Hasegawa, S.; Horike, S.; Matsuda, R.; Furukawa, S.; Mochizuki, K.; Kinoshita, Y.; Kitagawa, S. *J. Am. Chem. Soc.* **2007**, *129*, 2607–2614.
(18) Horike, S.; Dinca, D.; Tamaki, K.; Long, J. R. *J. Am. Chem. Soc.* **2008**, *130*, 5854–5855.

(19) Kaye, S. S.; Long, J. R. *J. Am. Chem. Soc.* **2008**, *130*, 806–807.
(20) Swanson, C. H.; Shaikh, H. A.; Rogow, D. L.; Oliver, A. G.; Campana, C. F.; Oliver, S. R. J. *J. Am. Chem. Soc.* **2008**, *130*, 11737–11741.
(21) Bauer, C. A.; Timofeeva, T. V.; Settersten, T. B.; Patterson, B. D.; Liu, V. H.; Simmons, B. A.; Allendorf, M. D. *J. Am. Chem. Soc.* **2007**, *129*, 7136–7144.
(22) Rieter, W. J.; Taylor, K. M. L.; Lin, W. *J. Am. Chem. Soc.* **2007**, *129*, 9852–9853.
(23) Park, H. B.; Jung, C. H.; Lee, Y. M.; Hill, A. J.; Pas, S. J.; Mudie, S. T.; Van Wagner, E.; Freeman, B. D.; Cookson, D. J. *Science* **2007**, *318*, 254–258.
(24) Serre, C.; Mellot-Draznieks, C.; Surble, S.; Audebrand, N.; Filinchuk, Y.; Ferey, G. *Science* **2007**, *315*, 1828–1831.
(25) Shimomura, S.; Horike, S.; Matsuda, R.; Kitagawa, S. *J. Am. Chem. Soc.* **2007**, *129*, 10990–10991.
(26) Zhou, W.; Wu, H.; Yildirim, T.; Simpson, J. R.; Walker, A. R. H. *Phys. Rev. B* **2008**, *78*, 5.
(27) Goodwin, A. L.; Calleja, M.; Conterio, M. J.; Dove, M. T.; Evans, J. S. O.; Keen, D. A.; Peters, L.; Tucker, M. G. *Science* **2008**, *319*, 794–797.
(28) Wu, Y.; Kobayashi, A.; Halder, G. J.; Peterson, V. K.; Chapman, K. W.; Lock, N.; Southon, P. D.; Kepert, C. J. *Angew. Chem., Int. Ed.* **2008**, *47*, 8929–8932.
(29) Peterson, V. K.; Kearley, G. J.; Wu, Y.; Ramirez-Cuesta, A. J.; Kemner, E.; Kepert, C. J. *Angew. Chem.* **2010**, *49*, 585–588.
(30) Chapman, K. W.; Halder, G. J.; Chupas, P. J. *J. Am. Chem. Soc.* **2008**, *130*, 10524–10526.
(31) Chui, S. S.-Y.; Lo, S. M.-F.; Charmant, J. P. H.; Orpen, A. G.; Williams, I. D. *Science* **1999**, *283*, 1148–1150.
(32) Alaerts, L.; Seguin, E.; Poelman, H.; Thibault-Starzyk, F.; Jacobs, P. A.; De Vos, D. E. *Chem.—Eur. J.* **2006**, *12*, 7353–7363.
(33) Schlichte, K.; Kratzke, T.; Kaskel, S. *Microporous Mesoporous Mater.* **2004**, *73*, 81–88.
(34) Dathe, H.; Peringer, E.; Roberts, V.; Jentys, A.; Lercher, J. A. *C. R. Chim.* **2005**, *8*, 753–763.
(35) Hartmann, M.; Kunz, S.; Himsl, D.; Tangermann, O.; Ernst, S.; Wagener, A. *Langmuir* **2008**, *24*, 8634–8642.
(36) Karra, J. R.; Walton, K. S. *Langmuir* **2008**, *24*, 8620–8626.
(37) Mueller, U.; Schuber, M.; Teich, F.; Puetter, H.; Schierle-Arndt, K.; Pastr, J. *J. Mater. Chem.* **2006**, *16*, 626–636.
(38) Wang, Q. M.; Shen, D. M.; Bulow, M.; Lau, M. L.; Deng, S. G.; Fitch, F. R.; Lemcoff, N. O.; Semanscin, J. *Microporous Mesoporous Mater.* **2002**, *55*, 217–230.
(39) Wang, S. Y.; Yang, Q. Y.; Zhong, C. L. *Sep. Purif. Technol.* **2008**, *60*, 30–35.
(40) Yang, Q. Y.; Zhong, C. L. *J. Phys. Chem. B* **2006**, *110*, 17776–17783.
(41) Zacher, D.; Baunemann, A.; Hermes, S.; Fischer, R. A. *J. Mater. Chem.* **2007**, *17*, 2785–2792.
(42) Bordiga, S.; Regli, L.; Bonino, F.; Groppo, E.; Lamberti, C.; Xiao, B.; Wheatley, P. S.; Morris, R. E.; Zecchina, A. *Phys. Chem. Chem. Phys.* **2007**, *9*, 2676–2685.
(43) Krawiec, P.; Kramer, M.; Sabo, M.; Kunschke, R.; Fröde, H.; Kaskel, S. *Adv. Eng. Mater.* **2006**, *8*, 293–296.
(44) Krungleviciute, V.; Lask, K.; Heroux, L.; Migone, A. D.; Lee, J. Y.; Li, J.; Skoulidas, A. *Langmuir* **2007**, *23*, 3106–3109.
(45) Liu, Y.; Brown, C. M.; Neumann, D. A.; Peterson, V. K.; Kepert, C. J. *J. Alloys Compd.* **2007**, *446−447*, 385–388.
(46) Panella, B.; Hirscher, M.; Putter, H.; Muller, U. *Adv. Funct. Mater.* **2006**, *16*, 520–524.
(47) Peterson, V. K.; Liu, Y.; Brown, C. M.; Kepert, C. J. *J. Am. Chem. Soc.* **2006**, *128*, 15578–15579.
(48) Prestipino, C.; Regli, L.; Vitillo, J. G.; Bonino, F.; Damin, A.; Lamberti, C.; Zecchina, A.; Solari, P. L.; Kongshaug, K. O.; Bordiga, S. *Chem. Mater.* **2006**, *18*, 1337–1346.
(49) Senkovska, I.; Kaskel, S. *Microporous Mesoporous Mater.* **2008**, *112*, 108–115.
(50) Vishnyakov, A.; Ravikovitch, P. I.; Neimark, A. V.; Bulow, M.; Wang, Q. M. *Nano Lett.* **2003**, *3*, 713–718.
(51) Vitillo, J. G.; Regli, L.; Chavan, S.; Ricchiardi, G.; Spoto, G.; Dietzel, P. D. C.; Bordiga, S.; Zecchina, A. *J. Am. Chem. Soc.* **2008**, *130*, 8386–8396.
(52) Bohlmann, W.; Poppl, A.; Sabo, M.; Kaskel, S. *J. Phys. Chem. B* **2006**, *110*, 20177–20181.
(53) Poppl, A.; Kunz, S.; Himsl, D.; Hartmann, M. *J. Phys. Chem. C* **2008**, *112*, 2678–2684.
(54) Zhang, X. X.; Chui, S. S. Y.; Williams, I. D. *J. Appl. Phys.* **2000**, *87*, 6007–6009.
(55) Biemmi, E.; Scherb, C.; Bein, T. *J. Am. Chem. Soc.* **2007**, *129*, 8054–+.
(56) Che, G. B.; Liu, C. B.; Liu, B.; Wang, Q. W.; Xu, Z. L. *CrystEngComm* **2008**, *10*, 184–191.
(57) Gascon, J.; Aguado, S.; Kapteijn, F. *Microporous Mesoporous Mater.* **2008**, *113*, 132–138.
(58) Liu, J. C.; Culp, J. T.; Natesakhawat, S.; Bockrath, B. C.; Zande, B.; Sankar, S. G.; Garberoglio, G.; Johnson, J. K. *J. Phys. Chem. C* **2007**, *111*, 9305–9313.
(59) Shekhah, C.; Wang, H.; Kowarik, S.; Schreiber, F.; Paulus, M.; Tolan, M.; Sternemann, C.; Evers, F.; Zacher, D.; Fischer, R. A.; Woll, C. *J. Am. Chem. Soc.* **2007**, *129*, 15118–+.
(60) Shoaee, M.; Agger, J. R.; Anderson, M. W.; Attfield, M. P. *CrystEngComm* **2008**, *10*, 646–648.
(61) Walker, A. M.; Slater, B. *CrystEngComm* **2008**, *10*, 790–791.
(62) Brown, C. M.; Liu, Y.; Yildirim, T.; Peterson, V. K.; Kepert, C. J. *Nanotechnology* **2009**, 20.
(63) Larson, A. C.; VonDreele, R. B. *Los Alamos National Laboratory Report* 2000, *LAUR*, 86-748.
(64) Toby, B. H. *J. Appl. Crystallogr.* **2001**, *34*, 210–213.
(65) Nijem, N.; Veyan, J. F.; Kong, L. Z.; Wu, H. H.; Zhao, Y. G.; Li, J.; Langreth, D. C.; Chabal, Y. J. *J. Am. Chem. Soc.* **2010**, *132*, 14834–14848.
(66) Liu, Y.; Kabbour, H.; Brown, C. M.; Neumann, D. A.; Ahn, C. C. *Langmuir* **2008**, *24*, 4772–4777.
(67) Patchkovskii, S.; Tse, J. S. *Proc. Natl. Acad. Sci. U.S.A.* **2003**, *100*, 14645–14650.
(68) Clare, B. W.; Kepert, D. L. *J. Math. Chem.* **1991**, *6*, 325–349.
(69) Yildirim, T.; Hartman, M. R. *Phys. Rev. Lett.* **2005**, 95.
(70) Poirier, E.; Dailly, A. *Langmuir* **2009**, *25*, 12169–12176.